

A CAD System for Developing Chemical Sensor-Based Microsystems with an ISFET-CMOS Compatible Technology

Sergio Martinoia, Leandro Lorenzelli, Giuseppe Massobrio,
Benno Margesin¹ and Alberto Lui¹

Department of Biophysical and Electronic Engineering (DIBE)
University of Genova, Via all'Opera Pia 11/A - 16145 Genova - Italy

¹Microsensor and System Integration Division
IRST/ITC - Via Sommariva, Pantè di Povo 38050 Trento - Italy

(Received March 29, 1999; accepted August 13, 1999)

Key words: ISFET microsystem, CAD system, ISFET/CMNOS technology, BIOSPICE

A CAD system, which makes use of an *ad hoc* technology [ISFET/CMNOS (ion-sensitive field-effect transistor/complementary metal nitride-oxide semiconductor) technology] for fabricating ISFET-based microsystems, has been developed. This technology combines ISFET fabrication technology and CMOS IC processes. To test it, we designed and built a microsystem consisting of three blocks (sensor, amplifier, and test structures) which allows us to check the electrochemical characteristics of the ISFET-based sensor, to evaluate the response of the microsystem under different measurement conditions, and to extract the parameters for BIOSPICE. The extraction of electrical and chemical parameters necessary to simulate the sensor behavior and to optimize the circuit design represents the basic and fundamental link between design and manufacturing. The CAD system developed can be considered a general purpose tool for designing integrated and «intelligent» sensing probes based on ISFET sensors. Similar microsystems can be used for any biomedical, environmental and biotechnological applications where slight variations around a static pH value are expected and miniaturization is required.

1. Introduction

Because of its characteristics of miniaturization and integration, the ion-sensitive field-effect transistor (ISFET) is a potential candidate for the low-cost mass fabrication of multisensor chips containing an array of chemically sensitive devices. Thus, by developing a CAD system which makes use of an *ad hoc* technology, it becomes feasible to realize increasingly more sophisticated sensors with on-chip amplification, offset correction, and interference reduction circuits. However, the processes usually employed in fabricating the ISFET are not fully compatible with standard CMOS processes which use silicon dioxide as the gate dielectric layer and polysilicon gates to self-align source and drain regions. On the other hand, it is known that the ISFET needs a gate insulator exhibiting good chemical sensing properties which are achieved using materials such as Si_3N_4 , Al_2O_3 and Ta_2O_5 .

Therefore, two different approaches may be followed. The first consists of modifying the ISFET structure to adapt it to the standard self-aligned poly-Si gate CMOS technology.⁽¹⁾ The second, which will be presented in the next sections, consists of keeping the ISFET fabrication technology and ensuring a partial compatibility to the CMOS IC process. The latter approach yielded a solution called ISFET/CMNOS technology.⁽²⁾ This technology has been used at IRST (IRST - Microsensors and System Integration Division, Trento, Italy) to fabricate microsystems containing ISFET-based pH sensors.

One of the main features of this technology is to make use of a double-layer gate insulator. In fact, an LPCVD (low-pressure chemical vapor deposition) silicon nitride film grown on the thermal gate oxide is an acceptable choice when CMOS and ISFET technologies must be compatible. Moreover, the deposition of this film is available as one of the standard passivation layers in IC technology, and, at the same time, it provides the ISFET a good proton sensitivity, good linearity, and acceptable stability and reliability. On the other hand, the high-temperature processing steps imposed by the Si_3N_4 deposition are not easy to accommodate to a standard poly-Si CMOS processing sequence.

To test the ISFET/CMNOS technology, we designed and realized a microsystem consisting of three blocks (sensor, amplifier and test structures) which allows us to check the electrochemical characteristics of the ISFET-based pH sensor, to evaluate the response of the microsystem under different measurement conditions, and to extract the parameters to be used with the simulation program BIOSPICE.⁽³⁻⁵⁾ The extraction of the electrical and chemical parameters necessary to simulate the sensor behavior and to optimize the circuit design represents, in the test plan of Fig. 1, the basic and fundamental link between design and manufacturing.

2. Simulation Tools

The ISFET is a MOSFET-based device (i.e., a MOSFET without the gate metallization) which uses an exposed gate insulator to measure ion concentrations or local changes in charge densities in electrolyte solutions.

The response of the ISFET to H^+ concentration (pH) is commonly explained using so-

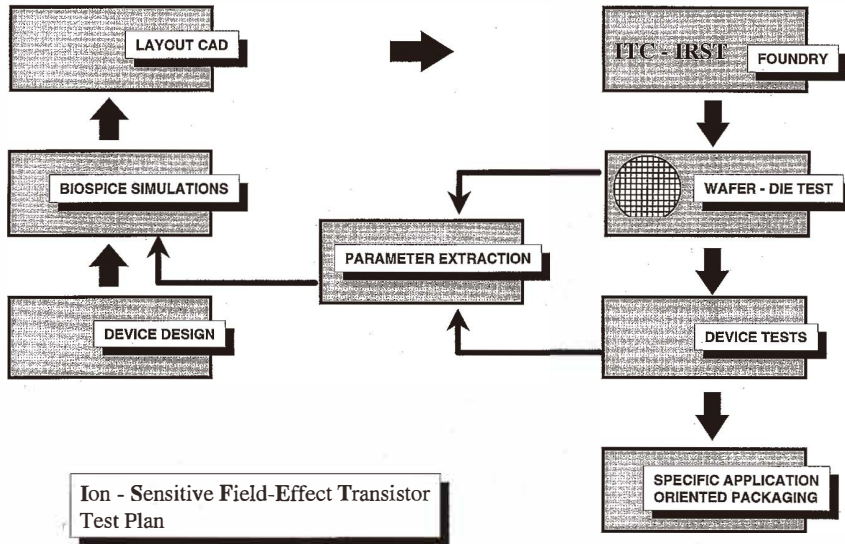


Fig. 1. Test plan for ISFET-based system design and fabrication.

called site-binding theory, which describes the charging mechanism of an oxide as the equilibrium between surface groups and H^+ ions in the bulk of the solution. This theory, together with the Gouy-Chapman-Stern model of the potential profile in the electrolyte and with the MOSFET physics, gives a complete description of the ISFET.

As a result, a set of equations is derived and introduced into BIOSPICE to predict the pH sensitivity and the dependence on the physico-chemical parameters of the ISFET. Typical insulator layers used are Al_2O_3 , Si_3N_4 and Ta_2O_5 . The model also takes into account non-ideal effects such as drift, hysteresis, and the case of partial insensitivity to pH, i.e., reference field-effect transistor (REFET). A detailed analysis of the ISFET model implemented in BIOSPICE can be found in references.⁽⁴⁻⁶⁾

The goal of the model is to obtain a relationship between pH and the electrolyte-insulator potential φ_{eo} which appears in the threshold voltage expression of the ISFET, i.e.:

$$V_{th}(\text{ISFET}) = (E_{ref} + \varphi_{lj}) - (\varphi_{eo}(\text{pH}) - \chi_{eo}) - \left(\frac{Q_{ss} + Q_{sc}}{C_{ox}} - 2\varphi_f + \frac{\phi_s}{q} \right)$$

This equation includes terms derived from MOSFET theory as well as terms that are electrochemical in nature. More specifically, φ_f is the Fermi potential of the semiconductor, Q_{ss} is the fixed surface-state charge density at the insulator-semiconductor interface, Q_{sc} is the semiconductor surface depletion region charge density, C_{ox} is the insulator capacitance per unit area, $E_{ref} = (E_{ref} + E_{abs})$ is the potential of the reference electrode, φ_{lj} is the potential difference between the reference solution and electrolyte, φ_{eo} is the potential

of the electrolyte-insulator interface which determines the ISFET sensitivity to protons, χ_{eo} is the electrolyte-insulator surface dipole potential, and ϕ_s is the semiconductor work function. The equations formulated to obtain ϕ_{eo} have been implemented into BIOSPICE by modifying some subroutines of the original SPICE and introducing new ones. Recently, the models have also been updated to simulate the sensor behavior under temperature variations.⁽⁷⁾ In particular, we have implemented into BIOSPICE the equations that describe the temperature-dependence of the physico-chemical parameters of the ISFET, while neglecting the temperature-dependent parameters of the MOSFET (modified to form the basis of the ISFET) already present in the original version of SPICE. Most of the parameters that determine the temperature-dependence of the ISFET are contained in the expression of the threshold voltage of the device.

3. Microsystem Design

As stated in the Introduction, the microsystem consists of three blocks, each respectively devoted to test the electrochemical characteristics of the sensor, the signal conditioning circuit performance and to evaluate the ISFET/CMNOS process parameters.

The microsystem was preliminarily designed using BIOSPICE⁽⁵⁾ and an ISFET model and parameter values adapted from the literature. At the end of the fabrication process, parameter extraction procedures and the comparison between the estimated electrochemical behavior and the actual experimental results were used to optimize the values of parameters in the ISFET model and to close the test plan loop shown in Fig. 1. The physical layout of the microsystem was drawn using the MAGIC (version 6.0) CAD program.

Figure 2(a) shows the basic block diagram, i.e.:

1) Sensor block

It consists of one ISFET-based pH sensor (an Si_3N_4 -gate ISFET, from here on simply referred to as ISFET) and two Aluminum-gate *n*-channel MOSFETs (from here on simply referred to as ALUFETs) with the same geometry as the ISFET.

As far as this block is concerned, the main difference between the ISFET and ALUFET consists of the method of contacting the source and drain regions, in addition to the difference in materials of the gates (and hence their work functions). In fact, in a standard ALUFET, source and drain regions are connected to outer devices by aluminum contacts evaporated near the gate region. On the contrary, in an ISFET, the aluminum contact area is placed several millimeters away from the gate region to prevent possible contacts between the electrolyte solution and the metal source and drain regions.

2) Signal conditioning block

The signal conditioning block consists of a current source and a current mirror connected to a pair of matched ISFETs and ALUFETs resulting in a differential stage. Three output stages, i.e., a CMOS output stage, an *n*-channel MOSFET output stage and a double *n*-channel MOSFET output stage, which can be separately selected, are also available on the same chip. An additional ALUFET with the same geometry as the ISFET is provided to test the electronics before the wafer is cut. When the ISFET is operating, this additional ALUFET can be used as a temperature sensor.

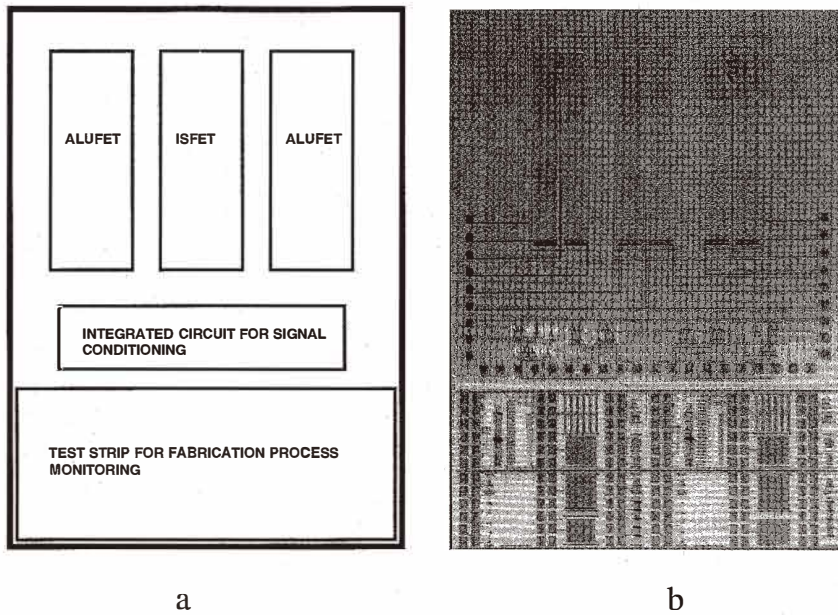


Fig. 2. (a) Basic block diagram of the microsystem chip; (b) fabricated chip.

As an example, Fig. 3 shows the circuit scheme of the differential stage coupled to the CMOS output stage. The two complementary MOSFETs of the output stage have been designed to work in saturation and to exhibit a gain of about 20.

3) Test strip block

This block includes 47 test structures of different sizes, i.e., capacitors, resistors, diodes, *p*-channel MOSFETs and *n*-channel MOSFETs, and it is devoted to technological evaluation, parameter extraction for BIOSPICE, and fabrication process monitoring.

Figure 2(b) shows the complete fabricated microsystem chip that follows the block diagram of Fig. 2(a). The dimensions of ISFET and ALUFETs are listed in Table 1.

Table 1.
ISFET-ALUFET geometrical parameters.

ISFET	AD=AS=22,050 μm^2	PD=PS=770 μm	L=36 μm	W=804 μm	NRD=NRS=8.5
ALUFET	AD=AS=22,050 μm^2	PD=PS=770 μm	L=36 μm	W=804 μm	NRD=NRS=8.5

Here, AD (AS) and PD (PS) are the drain (source) area and perimeter, respectively; *W* and *L* are the channel width and length, respectively; NRD (NRS) are the number of squares in the drain (source) regions, which are used to calculate the actual drain and source resistances (*R_D* and *R_S*) via the sheet resistance (*R_{SH}*). The parameter keywords are those used in BIOSPICE. The *W/L* ratio was chosen to obtain a high channel conductance value.

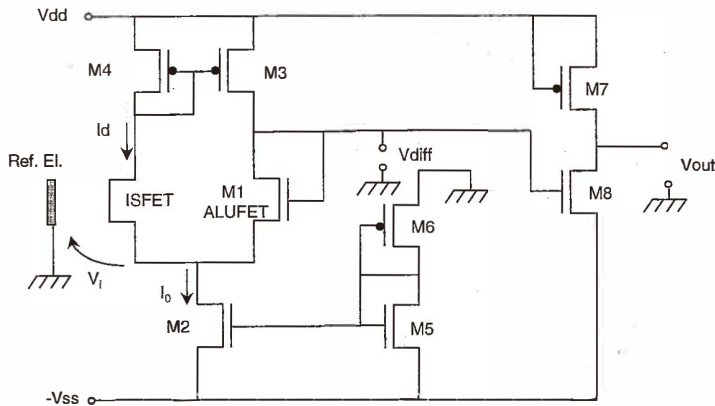


Fig. 3. Schematic of the signal conditioning block with the CMOS output stage.

4. ISFET/CMNOS Technology

The main goal of the proposed ISFET/CMNOS technology is to make CMOS technology compatible with the ISFET fabrication process. Thus, a 4 micron Al-gate *p*-well CMNOS technology, which uses an oxide/nitride double layer as a gate dielectric, was developed.

The fabrication process is basically a conventional *p*-well metal-gate CMOS process with added field channel stop implants for a better device isolation and to separate threshold adjustment implants for *p*- and *n*-channel MOSFETs. The chemical sensing layer is made of stoichiometric Si_3N_4 deposited at 775°C in an LPCVD system (ASM DFR210) using ammonia and dichlorosilane in a 4:1 flow ratio. The main characteristic of this technology consists of using the double layer $\text{Si}_3\text{N}_4/\text{SiO}_2$ as the insulator for fabricating both the ISFET sensor and all the MOSFETs of the integrated electronics.

Figure 4 shows a cross section of the fabricated ISFET sensor integrated with *p*-MOSFETs and *n*-MOSFETs on the same chip.

In the current release of the fabrication process, the ISFET is considered as an Al-gate MOSFET without the gate metal with the same threshold adjustment as an *n*-channel Al-gate MOSFET.

Additional features with respect to conventional CMOS processes were implemented to optimize the performance of the fabricated devices. They involved improved impermeabilization (thicker passivation oxide), increased ESD (electrostatic discharge) immunity (thicker field and interdiffusion-metal oxide) and optimization of diode breakdown voltage, and contact resistance (adjustment of the junction depths and surface doping diode concentration).⁽⁸⁾

The fabrication process is outlined in Table 2. The technology developed requires 13 lithography steps and a total of seven implants. Appropriate annealings, not listed in Table

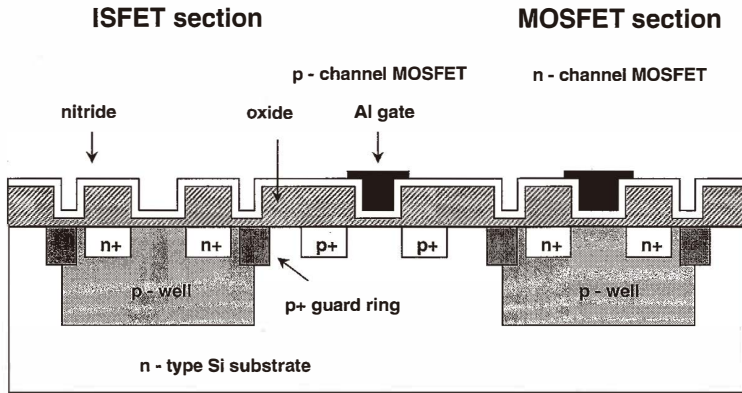


Fig. 4. Cross section of the ISFET sensor with *p*-channel MOSFETs and *n*-channel MOSFETs.

2, were added to stabilize the oxide-nitride layer, to reduce charge-trap densities at Si-SiO₂ and SiO₂-Si₃N₄ interfaces, and to improve the pH sensitivity of the exposed silicon nitride surface. The final target specifications of the revised process are summarized in Table 3.

Several runs were carried out to test the technology developed. The parametric test results performed on each run confirmed the stability and reproducibility of the process.

5. Process Parameter Extraction

The test structures devoted to electrical testing were measured using an automated parametric test system, and a complete set of both geometrical and electrical parameters was extracted by standard methods.⁽⁹⁾ From the input and output characteristics of MOSFETs, with different calibrated channel widths (W) and lengths (L), a set of BIOSPICE parameters was obtained. These parameters were utilized to complete the feedback loop (see Fig. 1) between measurements and simulation results. The extracted parameters are listed in Table 4.

Finally, measured and simulated MOSFET characteristics were compared to verify the quality of the parameter extraction procedures for BIOSPICE.

As an example, the input characteristics of two *n*-channel MOSFETs with the same channel lengths ($L=15\ \mu\text{m}$) but different widths ($W_1=15\ \mu\text{m}$ and $W_2=84\ \mu\text{m}$) were simulated with BIOSPICE (see Fig. 5). The simulation results were compared to measured curves. BIOSPICE simulations of test MOSFETs are the necessary starting point before analyzing the electrochemical behavior of the ISFET realized with the proposed technology.

Table 2.
ISFET/CMNOS process outline.

Substrate: <i>n</i> -type Si, (100), CZ 8 Ωcm	
1st photostep:	p-well
1st implant:	Boron; E=100 keV; D=4.5·10 ¹² /cm ² through screen oxide
<i>p</i> -well drive in:	T=1150°C; t=15 h; dry
2nd photostep:	p+ guard ring
2nd implant:	Boron; E=120 keV; D=1.0·10 ¹³ /cm ² through screen oxide
3rd photostep:	n-substrate active area
3rd implant:	Phosphorus; E=100 keV; D=4.5·10 ¹² /cm ² through screen oxide
<i>field oxide growth</i>	T=975°C; t=9 h steam; 1150 nm
4th photostep:	define diodes
5th photostep:	select p+ regions (guard ring)
4th implant:	BF ₂ , E=80 keV, D=5.0·10 ¹⁵ /cm ² through screen oxide
<i>first diode drive:</i>	T=975°C, t=80 min; inert ambient
6th photostep:	select n+ regions
5th implant:	BF ₂ , E=80 keV, D=5.0·10 ¹⁵ /cm ² through screen oxide
<i>second diode drive:</i>	T=1150°C, t=1 h; inert ambient
7th photostep:	define gate area
8th photostep:	p-select
6th implant:	BF ₂ , E=50 keV, D=1.0·10 ¹² /cm ² through sacrificial oxide
9th photostep:	n-select
7th implant:	Boron; E=30 keV; D=1.0·10 ¹² /cm ² through sacrificial oxide
10th photostep:	p & n select
<i>gate oxide growth</i>	T=975°C; t=30 min; 30 nm
<i>LPCVD nitride deposition:</i>	T=795°C; t=30 min; 100 nm
11th photostep:	contact opening
<i>Al sputter deposition:</i>	1200 nm
12th photostep:	define metal
<i>LTO Deposition:</i>	T=430°C; t=30 min; 500 nm
13th photostep:	define overglass
<i>Contact sintering</i>	T=400°C; t=5 min

As temperature affects ISFET and MOSFET parameters and performance,^(7,10) a set of measurements and simulations at temperatures in the range of 20–140 °C were also performed on *n*-channel and *p*-channel MOSFETs to test the dependence of their threshold voltages on the operating temperatures (Fig. 6). The different behaviors and degrees of accuracy in the simulation results are mainly due to two factors:

1) the *n*-channel MOSFET was built in a more heavily doped *p*-well, whereas the *p*-channel MOSFET was built in a lightly doped substrate;⁽¹¹⁾

Table 3.
Target process specifications.

Single well, 4 micron, single metal gate CMOS process	
Gate oxide thickness	33 nm
Field oxide thickness	1,700 nm
Nitride thickness	100 nm
PMOS, NMOS, threshold voltages	1.0 V
Field threshold voltages	> 20 V
Interdiffusion-metal dielectric (TEOS undoped)	400 nm
Metal (pure Al) thickness	1,200 nm
Substrate doping concentration	$4.5 \times 10^{14} \text{ cm}^{-3}$
Well surface doping concentration	$1.0 \times 10^{16} \text{ cm}^{-3}$
p+ junction depth	$3.0 \times 10^{-6} \text{ m}$
n+ junction depth	$2.2 \times 10^{-6} \text{ m}$
p-well depth	$7.0 \times 10^{-6} \text{ m}$
Junction breakdown voltages	> 22 V
PMOS zero field mobility	$410 \text{ cm}^2/\text{V}\cdot\text{s}$
NMOS zero field mobility	$610 \text{ cm}^2/\text{V}\cdot\text{s}$
p+ sheet resistance	35 Ω/sq
n+ sheet resistance	12 Ω/sq
p-well sheet resistance	4,000 Ω/sq
Metal sheet resistance	30 m Ω/sq
p+ contact resistance	230 Ω/cont
n+ contact resistance	230 Ω/cont

Table 4.
Geometrical and electrical parameters. Their keywords are those used in BIOSPICE .MODEL statement.

Parameters	NMOS		PMOS	
CGSO [F/m]	1.18	$\pm 0.011 \times 10^{-9}$	1.24	$\pm 0.02 \times 10^{-9}$
CGDO [F/m]	1.18	$\pm 0.011 \times 10^{-9}$	1.24	$\pm 0.02 \times 10^{-9}$
CGBO [F/m]	2.76	$\pm -1 \times 10^{-10}$	2.76	$\pm -1 \times 10^{-10}$
VTO [V]	1.	± -0.1	-1	± -0.1
RSH [(/sq)]	350	± 1.6	1140	± 0.13
TOX [m]	8.39	$\pm 0.05 \times 10^{-8}$	8.52	$\pm 0.08 \times 10^{-8}$
UO [cm^2/Vs]	533	± 9	233	± 3
UCRIT [V/cm]	1.89	$\pm 0.15 \times 10^4$	1.16	$\pm 0.10 \times 10^5$
UEXP	0.0512	± 0.0010	0.14	± 0.001
UTRA	0	$\pm -$	0	$\pm -$
NSUB [cm^{-3}]	2.8	$\pm 0.3 \times 10^{16}$	1.22	$\pm 0.11 \times 10^{15}$
NFS [cm^{-2}]	1.23	$\pm 0.07 \times 10^{12}$	2.89	$\pm 0.4 \times 10^{11}$
NEFF	0.57	± 0.03	3.98	± 0.5
VMAX [m/s]	5.53	$\pm 0.15 \times 10^4$	1.81	$\pm 0.04 \times 10^4$
DELTA	6.5	± 0.2	4.3	± 0.2
LD [m]	2.92	$\pm 0.11 \times 10^{-6}$	3.07	$\pm 0.03 \times 10^{-6}$
WD [m]	0.14	$\pm 0.14 \times 10^{-6}$	1.33	$\pm 0.03 \times 10^{-6}$
XJ [m]	3	$\pm 0.3 \times 10^{-7}$	6.7	$\pm 1.3 \times 10^{-7}$
CJ [F/m^2]	2.24	$\pm 0.009 \times 10^{-4}$	8.71	$\pm 0.4 \times 10^{-5}$
CJSW [F/m]	1.5	$\pm 0.02 \times 10^{-9}$	8.91	$\pm 0.2 \times 10^{-10}$
MJ	0.443	± 0.002	0.433	± 0.003
MJSW	0.378	± 0.004	0.335	± 0.0018
JS [A/m^2]	6.1	$\pm 1.2 \times 10^{-6}$	3	$\pm 2. \times 10^{-6}$
PB [V]	0.759	± 0.005	0.546	± 0.008

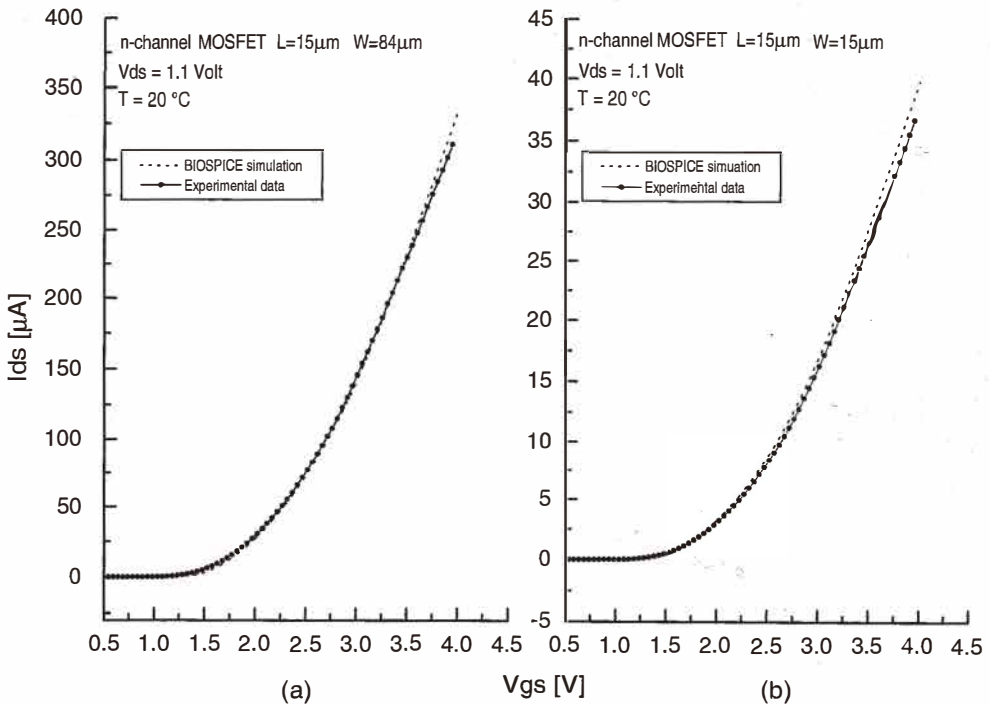


Fig. 5. Comparison between BIOSPICE simulation results and experimental measurements of input characteristics of an n -channel MOSFET with (a) $W/L = 84/15$, and (b) $W/L = 15/15$.

2) the n -channel MOSFET fabrication process can induce buried-channel effects which cause a threshold voltage shift, whereas in the p -channel MOSFET, some of these effects partially cancel each other.⁽¹²⁾

6. Electrochemical Tests of the Encapsulated Microsystem

Microsystems, i.e. ISFETs and their amplification circuits, were bonded and encapsulated onto a 40-pin DIL (dual in line) package. The encapsulated devices were tested to verify the correct behavior of the ISFET sensors under standard conditions. Hence, a set of electrochemical measurements were performed to verify the ISFET input and output characteristics, pH sensitivity, long-term drift and temperature dependence.

6.1 Single ISFET experimental measurements

An automatic test set-up devoted to electrochemical measurements was used to characterize the fabricated ISFET sensors. The test protocols was as follows:

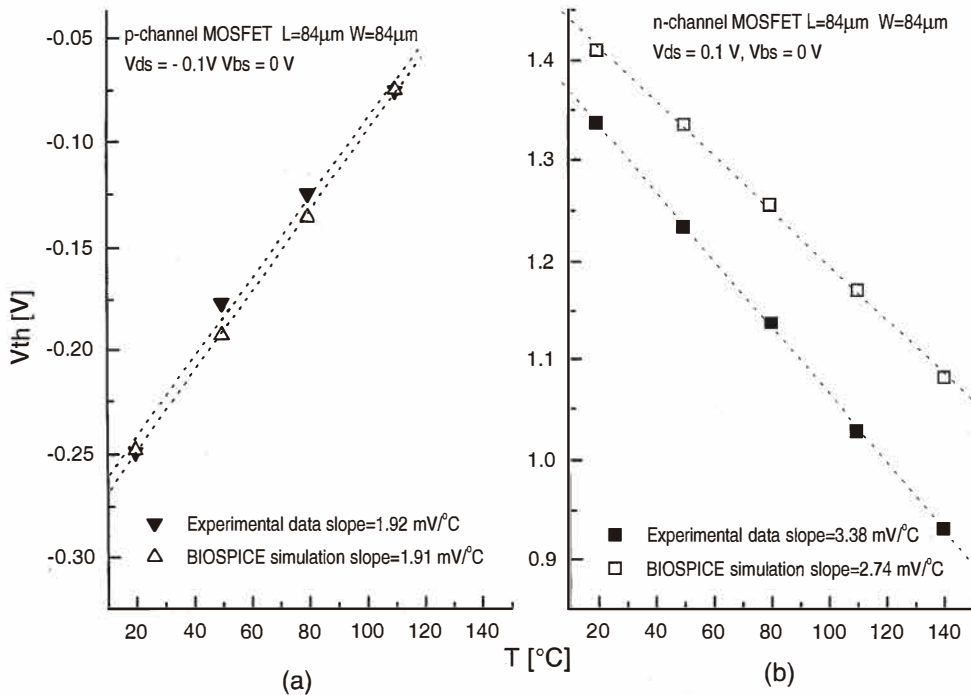


Fig. 6. Variations of the threshold voltage with temperature for (a) *p*-channel MOSFET, $W/L = 84/84$, and (b) *n*-channel MOSFET, $W/L = 84/84$.

surface sensor cleaning with HF 1:50;
 sensor conditioning in 100 mM of an NaCl solution for at least 10 h;
 I_{ds} vs V_{ds} , and I_{ds} vs V_{gs} curves in a pH buffer;
 pH sensitivity using buffers at different pHs (pH=4, pH=7, pH=10);
 temperature dependence (data not shown, see ref. (10));
 long-term drift measurements at constant I_{ds} and pH.

As an example, Fig. 7 shows the measured input characteristics at three pH values (measured sensitivity 57 mV/pH). Typical long-term drift curves are shown in Fig. 8 for a device at a constant pH = 7 (average measured drift 0.19 mV/h).

It should be noted that packaging, assembling and encapsulation procedures are critical steps for obtaining reliable sensors with reproducible performance. Repeated tests on several ISFETs obtained from the same wafer showed only negligible variations on the electrochemical behavior. Figure 9 shows the ISFET input characteristics at pH = 7 and $V_{ds} = 0.1\text{ V}$ for two fabrication runs (CF5 and CF8) which differ by a slight variation in the implant dose for threshold voltage adjustment. The effects of implant dose on the threshold voltage were also studied in *p*-channel and *n*-channel MOSFET test devices (data not shown).

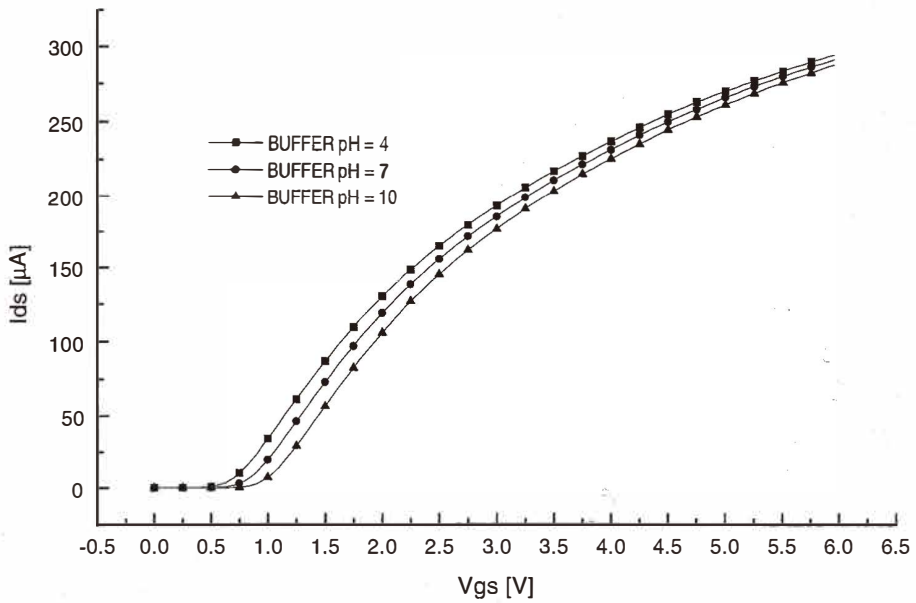


Fig. 7. ISFET input characteristics measured at different pH (4, 7, 10) and $V_{ds} = 0.5$ V.

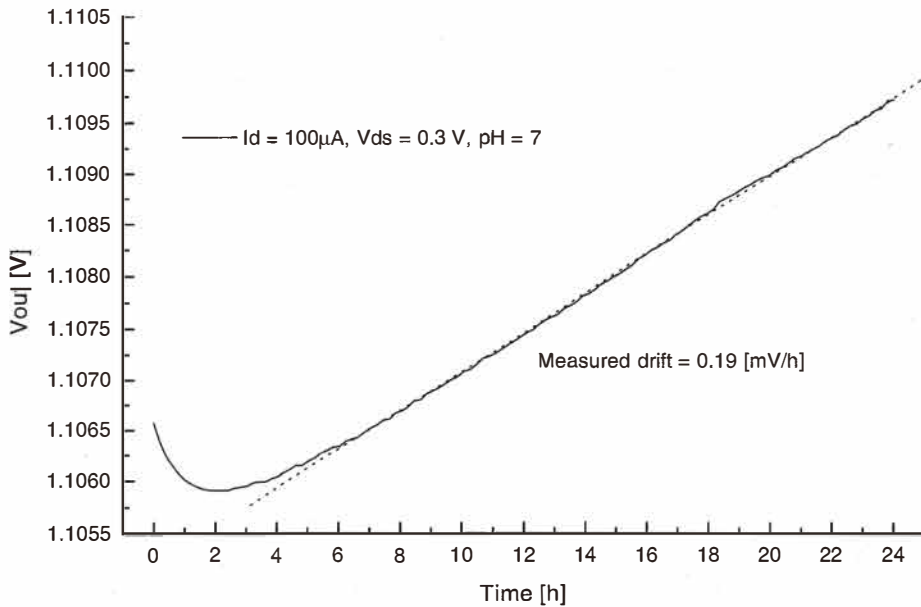


Fig. 8. Experimental results of a drift measurement at a constant pH = 7 and $V_{ds} = 0.3$ V.

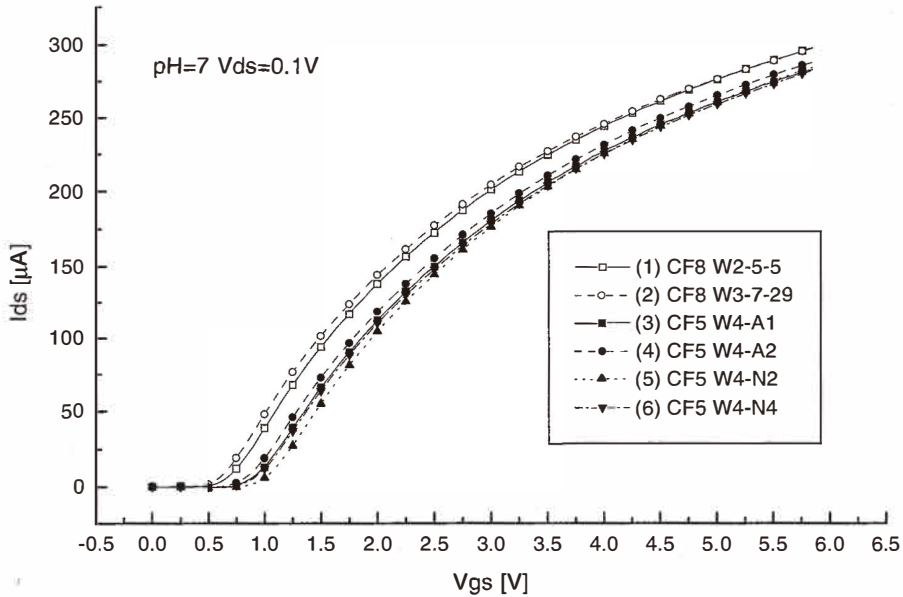


Fig. 9. ISFET input characteristics at pH = 7 and $V_{ds} = 0.1$ V for two technological runs (CF5 and CF8).

6.2 Microsystem experimental measurements

The functionality of the electronic circuit blocks was verified both on wafers and on the packaged devices. A preliminary chip characterization was performed directly on the wafer connecting the two ALUFETs as the input of the differential stage, and measuring, using a parametric test system, the transfer characteristics of the differential stage coupled to the output amplification circuit. The functionality of the electronic circuit blocks has also been verified on the packaged chip. In this case, the ISFET was one of the input transistors as shown in the circuit of Fig. 3. A protocol similar to that for the single ISFET electrochemical measurements was used (cf. section 6.1).

As an example, Fig. 10 shows the output voltage (V_{out}) of the differential stage coupled to the CMOS output stage as a function of the applied voltage V_{diff} at two bias voltage (V_{gs}) values applied to the output stage.

7. Microsystem Circuit Simulations

As already described (cf. section 3), the microsystem was designed using BIOSPICE, which has built-in models for ISFET-based sensors.^(4,5) BIOSPICE allowed us to simulate the ISFET behavior and the related integrated electronic circuits by specifying the electrochemical parameters together with the standard parameters for the MOSFET, which is the

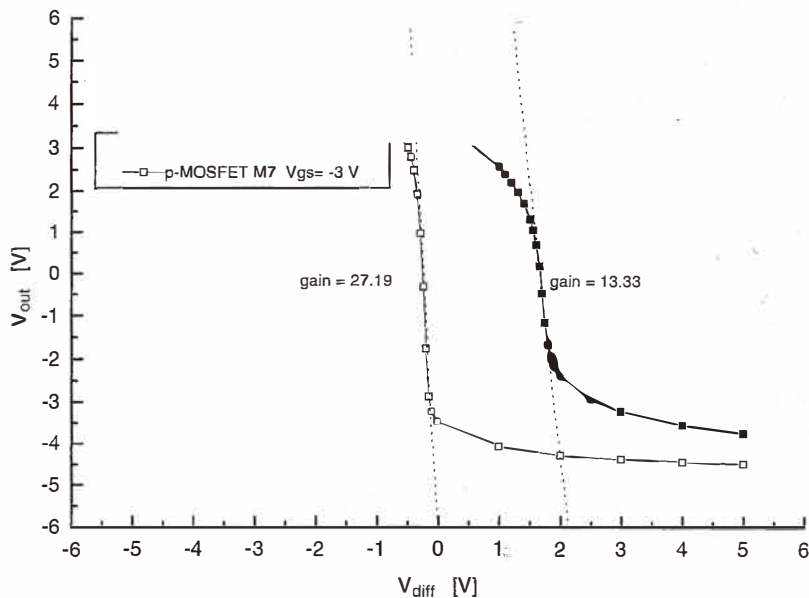


Fig. 10. Output voltage V_{out} of the differential stage coupled to the CMOS stage as a function of the differential input voltage V_{diff} .

starting structure of the ISFET.

At the end of the fabrication process, results of the BIOSPICE simulation were compared with the measured experimental data obtained from the encapsulated microsystem. To simulate the ISFET behavior, the parameter values listed in Table 5 were used for the .MODEL statement of BIOSPICE. Some values of parameters were extracted by measuring test devices and other parameter values were estimated or obtained from the literature.

The differential stage in the follower configuration was simulated and compared with experimental data (see Fig. 11) at different pH values.

As an example, Fig. 12 shows the simulations of the differential stage coupled to the CMOS output stage at different pH values corresponding to the pH of the buffer solutions used in the experimental measurements. Apart from a slight offset, the CMOS output stage shows (when both p -channel and n -channel MOSFETs operate in saturation mode) a maximum gain value of 21.7 in accordance with the experimental results. As can be seen, the linearity interval of the amplifier is restricted to a narrow range around the physiological pH.

The BIOSPICE model has been extensively validated,^(4,5,7,13) and actual deviations of the simulated results from the measured ones have to be related to the non-optimized protocol used for extracting the model parameter values.

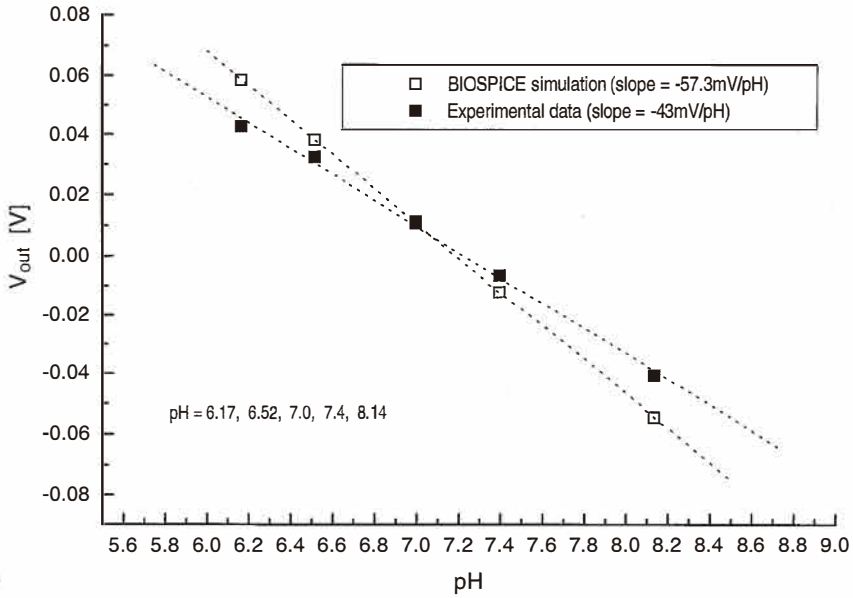


Fig. 11. Measured and simulated characteristics of the fabricated ISFET-based microsystem in the follower configuration as a function of different pH values of the electrolyte solution.

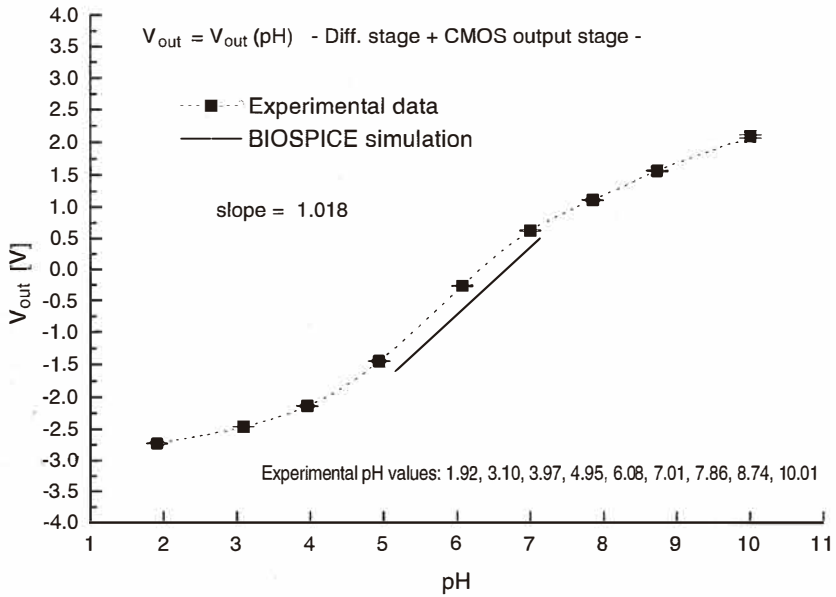


Fig. 12. Comparison between measured and simulated output voltage V_{out} of the ISFET-ALUFET differential stage coupled to the CMOS output stage as a function of the pH value of the solution.

Table 5.
ISFET electrochemical parameters used in the .MODEL statement of BIOSPICE.

BIOSPICE Keywords		Definitions of parameters
ZTOXN = 100 N	t_{ox2}	Si_3N_4 thickness (m);
ZEPSOX = 66.4 P	ϵ_{ox2}	Si_3N_4 dielectric constant (F/m);
ZEPSIL = 0.0	η	Fraction of buried binding sites (sites/cm ²);
ZNKAP = 0.1 N	$K_{\text{N}+}$	Primary amine dissociation constant (mol/l);
ZPH = 7.0	pH	pH operating point;
ZDEFF = 1	D	Effective diffusion coefficient (cm ² /s);
ZAKAP = 15.8	K_+	Dissociation constant for positive silanol groups (mol/l);
ZBKAP = 63.1 N	K	Dissociation constant for negative silanol groups (mol/l);
ZSCON = 0.1	C_0	Ion concentration in the electrolyte (mol/l);
ZNOX = 3.E14	N_{sil}	Silanol surface site density (sites/cm ²);
ZNNIT = 2.E14	N_{nit}	Primary amine surface site density (sites/cm ²);
ZEREL = 0.205	E_{rel}	Reference electrode potential;
ZCHIEO = 50 M	χ_e	Surface dipole potential;
ZPHLJ = 3 M	ϕ_{ij}	Liquid-junction potential difference between the reference solution and the electrolyte.

8. Conclusions

The test plan of Fig. 1 has been used to realize a CAD system for developing reliable and efficient sensor-based microsystems for specific applications.

The ISFET/CMNOS technology developed has benefited from modern design methodologies (e.g., *ad-hoc* developed CAD simulation tools, on-wafer test parameter structure, single die testing) and demonstrates the possibility of designing and fabricating miniature integrated systems in which the sensing element is directly integrated with the signal conditioning electronics. Specific applications in biomedical and environmental fields can be envisaged. Some works on this topic have been carried out, namely, on-line detection of microorganisms in waters⁽¹³⁾ and on-line cell population metabolism monitoring.⁽¹⁴⁾

The CAD system developed can be considered a general purpose tool in designing integrated and «intelligent» sensing probes based on ISFET sensors. The developed microsystem can be utilized for biomedical, environmental and biotechnological applications where slight variations around a static pH value are expected and miniaturization is required.

The proposed design methodology (cf. test plan of Fig. 1) could be applied to other well-established or new ISFET-based sensor fabrication technologies (e.g., refs. (1,15–17)) resulting in enhanced quality of design and production.

Future works will be devoted to standardization and optimization of the parameter extraction procedures (especially for the values of electrochemical parameters) and to the implementation of «behavioral macromodels» which could be easily implemented into different commercial versions of SPICE (e.g., HSPICE, PSPICE, SPICE3).

Summarizing, we have developed an *ad hoc* technology (ISFET/CMNOS) and proposed a design methodology, both resulting in the realization of a CAD system for fabricating ISFET-based microsystems. However, this system has to be considered a prototype one which can obviously be optimized, not certainly as far as the model is concerned, but surely as far as some procedures for extracting technological (physical, chemical and geometrical) parameters are concerned.

References

- 1 L. Bousse, J. Shott and J. D. Meindl: IEEE Electron Device Lett. **9** (1988) 44.
- 2 A. Lavarian, A. Lui, B. Margesin, G. Soncini and V. Zanini: Proc. MIEL-SD 93 Conference, Bled Slovenia (1993).
- 3 G. Massobrio and P. Antognetti: Semiconductor Device Modeling with SPICE, 2nd ed. (McGraw Hill, New York, 1993).
- 4 M. Grattarola, G. Massobrio and S. Martinoia: IEEE Trans. Electron Devices ED-39 (1992) 813.
- 5 G. Massobrio, S. Martinoia and M. Grattarola: Sensors and Materials **6** (1994) 101.
- 6 S. Martinoia, G. Massobrio and M. Grattarola: Sensors and Actuators B-7 (1992) 561.
- 7 S. Martinoia, L. Lorenzelli, G. Massobrio, B. Margesin, A. Lui and P. Conci: Sensors and Actuators B **50** (1998) 60.
- 8 A. Lui, B. Margesin, V. Zanini, M. Zen, G. Soncini and S. Martinoia: Proc. ICMTS96, Trento (1996).
- 9 B. Margesin and V. Zanini: Experimental Process Parameters and Extrapolated Target Process Values for MGCMOS.B2bs Rev.B Processes, IRST, Trento, Italy (1996)
- 10 P. R. Barabash, R. S. C. Cobbold and W. B. Wlodarski: IEEE Trans. Electron Devices ED **34** (1987) 1271.
- 11 S. Cheng and P. Manos: IEEE Circuits and Devices Magazine, July 1989, 31.
- 12 F. M. Klassen and W. Hes: Solid State Electronics **29**(8) (1985) 787.
- 13 A. Cambiaso, S. Chiarugi, M. Grattarola, L. Lorenzelli, A. Lui, B. Margesin, S. Martinoia, V. Zanini and M. Zen: Sensors and Actuators B **24-25** (1996) 218.
- 14 European Patent application EP0870823A1: System for monitoring the metabolic activity of living cells.
- 15 A. Sibbald: Sensors and Actuators **7** (1985) 23.
- 16 R. E. G. van Hal, P. Bergveld and J. F. J. Engbersen: Sensors and Materials **8** (1996) 455.
- 17 T. C. W. Yeow, M. R. Haskard, D. E. Mulcahy, H. I. Seo and D. H. Kwon: Sensors and Actuators B **44** (1997).